From extraction of physiological features with dynamic μ-SPECT imaging to modelling of iodide biodistribution in stomach

Marine Breuilly, Kaouthar Chatti, Jacques Darcourt, Philippe Franken, Julien Guglielmi, Grégoire Malandain, Thierry Pourcher

From extraction of physiological features with dynamic μ-SPECT imaging to modelling of iodide biodistribution in stomach

Marine Breuilly[1,2], Kaouthar Chatti[2], Jacques Darcourt[2], Philippe Franken[2], Julien Guglielmi[2], Grégoire Malandain[3], and Thierry Pourcher[2]

[1] INRIA, 06900 Sophia Antipolis, France
[2] UMR E4320 UNS/CEA/CAL, TIRO-MATOs, 06107 Nice, France

Abstract. This study investigates the potential retention of iodide in the stomach, for a better understanding of the iodide biodistribution in the body and more precisely of its potential antiseptic role. To that end, we will study the uptake of the ^{99m}Tc-pertechnetate (an iodide analog) within the murine stomach observed thanks to a SPECT camera. The temporal evolution of the uptake is analysed thanks to a dedicated multi-compartment model. The addressed challenges consist in 1) estimating the time-activity curves for the different compartments, and 2) identifying the model parameters. Real experiments on different subjects demonstrate a quite good coherence of the computed parameters, and the computed parameter values suggested that there is some iodide retention in the stomach wall.

1 Introduction

This study investigates the potential retention of iodide in the stomach, for a better understanding of the iodide biodistribution in the body and more precisely of its potential antiseptic role. The role of iodide has been frequently studied in the thyroid, and complex models that describe iodide biodistribution exist. Besides, scintigraphy using ^{99m}Tc-pertechnetate represents a powerful tool for the study of iodide uptake in different organs of living animal models. Several studies analysed ^{99m}Tc-pertechnetate biodistribution in mice. Also, Lathrop et al. proposed a schematic representation of the whole-body murine ^{99m}Tc-pertechnetate biodistribution in [1], with temporal estimation of uptake or secretion of ^{99m}Tc-pertechnetate after an intravenous injection.

Uptake and kinetic of ^{99m}Tc-pertechnetate in stomach has been mentioned in a few papers [2]. However, no work have been done on the kinetic properties to determine if the upake is mainly in the stomach wall, or if the secretion and diffusion in the lumen are the most important processes. High uptake in the cells of the stomach wall is expected if the physiological role of the iodide accumulation in this organ is related to the antioxidant capacity of iodide. In this case, stomach accumulation aims to protect cells of the gastric mucosa that express the sodium iodide symporter (NIS) against other secreted reactive oxygen species

(ROS). In contrast, if the main compartment that accumulates iodide is the lumen, the physiological role of the stomach iodide is an antimicrobial defence. Indeed, oxidised iodine is a powerful antimicrobial agent that could eliminate bolus microbes. Kinetic studies on living animal should help to determine which of these two hypotheses is correct.

The presented work relies on a simplified two-compartment model of the stomach defined in Section 2.2. This model allows the distinction of the stomach wall from the cavity. In the literature, a few biodistribution studies have been conducted with compartmental analysis approaches on other organs than stomach using ET imaging and different radiopharmaceuticals: on the thyroid [3], on the heart [4] and on the brain [5,6].

The study is conducted on dynamic (3D+t) Single Photon Emission Computed Tomography (SPECT) images of mice where the progressive iodide uptake is observed (see Figure 2 in Section 2.3). The challenges addressed here are:

- to identify and to estimate the model input function (see Section 2.3);
- to estimate the time-activity curves (TAC) for each compartment of the model (see Section 2.3(a));
- to identify the model parameters (see Section 2.4(b)).

Finally, Section 3 presents the results and the characteristics of the model.

2 Method

2.1 Material

Animal model. Five C57Bl/7 mice, weighting around 20g, have been used for this study. The mice received a subcutaneous injection of 80 to 105 MBq in 400 μL of ^{99m}Tc-pertechnetate. Then, mice were anaesthetised with isoflurane just after injection and kept sedated during the whole imaging protocol. The animals were placed prone and freely breathing (without mechanical ventilation) on the bed. Animal housing and procedures were conducted according to the guidelines of the French Agriculture Ministry and were approved by the local ethics committee.

Dynamic SPECT imaging protocol. Dynamic μ-SPECT images were acquired with a dedicated small animal SPECT/CT scanner (eXplore speCZT CT 120, GE Healthcare, CA). Each dynamic image is composed of 12 or 19 frames, acquired every 5 to 10 minutes. The acquisition of each frame takes around three minutes for a total acquisition duration ranging from 90 to 135 minutes.

A monitoring system (BioVet, m2m Imaging Corp) was used with an abdominal pneumatic pressure sensor to control the respiratory rate of the animal. Anaesthetic gas rate was regularly controlled to keep the respiratory rate between 60 and 100 breaths per minute. Images are reconstructed using the basic non-gated 3D reconstruction scheme. The imaging field of view contains the whole stomach and heart. Additionally, images are corrected for the radioactive decay and converted into equivalent SUV.

2.2 Biodistribution modelling with compartmental analysis

Because the iodide kinetic is different in the two parts of the stomach (the wall and the cavity), we rely on a compartmental model to study our system. Thus, we proposed the two-compartment model of the ^{99m}Tc-pertechnetate biodistribution in the stomach shown in Figure 1. It is inspired from the whole-body model proposed in [1], restricted to the stomach.

We considered that the implicit assumptions related to compartmental analysis are valid (see [7]). For example, the representation of activity concentration in each compartment can be described by ODEs given in the Equations 1.

$$\begin{cases} \dot{x_1}(t) = -(k_{21} + k_{01})x_1(t) + k_{12}x_2(t) + k_{10}x_0(t) \\ \dot{x_2}(t) = k_{21}x_1(t) - (k_{12} + k_{02})x_2(t) \end{cases} \quad (1)$$

We have made several additional assumptions to obtain this simplified model:

- There is no iodide transport from the digestive system or other organs directly to the stomach; this approximation is valid because the kinetic of those exchanges is too slow relatively to the length of the observation.
- The system input is the blood.
- There might be leaks from stomach wall and cavity to the outside of the system, with transport parameters denoted k_{01} and k_{02}.
- The diffusion in the stomach cavity is not considered: as generally assumed in compartmental analysis, each compartment is considered to be homogeneous.

The objective is then to determine the transfer parameters k_{01}, k_{10}, k_{02}, k_{21}, k_{12}. In a preliminary step, we need to obtain the time-activity curves (TAC) for each of the involved compartments, i.e., the blood, the stomach wall, and the stomach cavity. These TACs are obtained by measuring the activity in volume of interest of dynamic SPECT images.

2.3 Time-activity curve extraction

Blood TAC: model input function. The blood time-activity curve is simply measured in the dynamic SPECT images. It corresponds to the average activity in a 3x3x3 mm^3 sphere located in the left ventricle. As the subcutaneous injection can be considered as an impulse, the blood TAC is expected to be a bolus. Therefore, each blood TAC can be approximated by a sum of two exponential functions with least square minimisation algorithm [8]. This approximated function will be used as the input of our compartmental model.

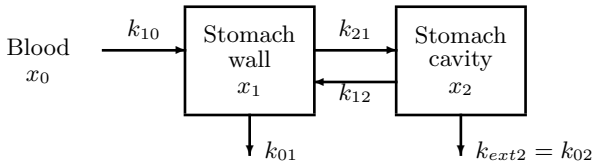

Fig. 1. Compartmental system after simplifications: two-compartment catenary system

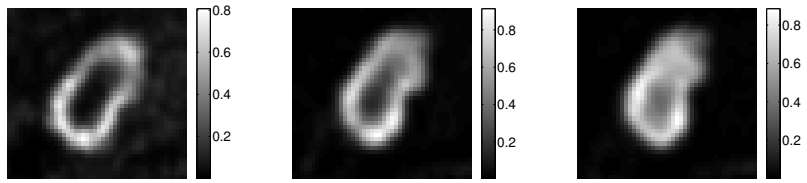

(a) Sagittal slice

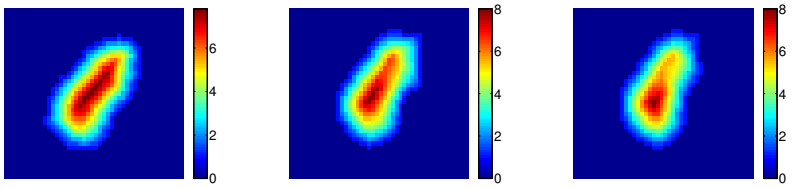

(b) Result of the Chamfer distance transformation on the stomach

Fig. 2. Temporal evolution of iodide uptake after subcutaneous injection of ^{99m}Tc-pertechnetate in subject #0835. Sample sagittal slice in the original image and after decomposition into layers are showed at 19 min, 54 min and 93 min after injection

Stomach wall and cavity TACs: model output functions. Concerning wall and cavity, it is not possible to measure easily and accurately the TACs. This is due to the motion (soft tissue deformation) and to the resolution of the images that does not allow the perfect segmentation of pure wall and pure cavity. Instead, each voxel is a mix between wall, cavity, and non diffusive tissues.

Segmentation of the whole stomach. The stomach is segmented independently in each frame of the 4D images by the Otsu method [9]. Then the largest connected component is selected and a morphological closing is applied. The resulting segmentation includes the whole stomach (wall + cavity).

Stomach decomposition into layers and layer TACs. A voxel-based analysis is not appropriate due to temporal evolution. Thus, a region-based analysis was chosen. The stomach was divided into layers. We made the assumption that the layers also refer to the same anatomical region. This kind of approach was already advocated by Zang et al. for functional MRI [10], where voxels are gathered into homogeneous regions.The layers are obtained by applying the 3D version for 5-7-11 Chamfer distance transformation. This transformation was chosen because it is the optimal approximation of the Euclidean distance [11]. Each stomach layer consists of the set of voxels that are equidistant to the outside of the stomach (i.e. the background). Figure 2 presents the result of the two first steps: the layer decomposition of the segmented stomach for subject #0835. Time-activity curves are obtained for each layer of the stomach, as shown in Figure 3 for subject #0530.

Mixing coefficients and compartment TACs computation. The compartment TACs are computed from the layer TACs. We assume that each layer in the

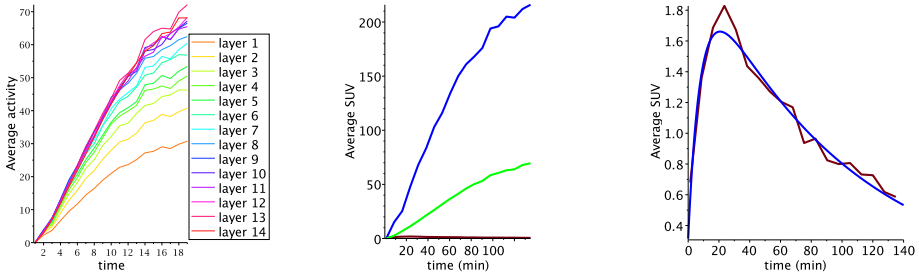

(a) First 14 layer TACs (b) Stomach wall (blue), cavity (green) and blood (red) TACs (c) Blood TAC (red) and its approximation (blue)

Fig. 3. Stomach wall and cavity TACs obtained from the layers TACs – subject #0530.

SPECT image is homogeneous and contributes to each compartment with a percentage, denoted *mixing coefficients* $\kappa_{i,j}$. The relation between the activity in the layers and in the compartments is described by: $L = K.C$, where K is the mixing coefficient matrix, L is the vector of activities in layers and C is the vector of activities in compartments. At each instant, the activity in the two compartments is obtained by computing the pseudo-inverse [12] of K: $\hat{C} = ({}^tK \cdot K)^{-1} \cdot {}^tK \cdot L$. To compute K, we first assumed that the volume ratio of each compartment composing each layer can be used as the mixing coefficients. The mixing coefficients have been estimated according to the anatomical spatial distribution of each compartment in a stomach immunohistochemistry (IHC) image. Then, the mixing coefficients of the first 14 layers were adjusted in order to minimise the sum of squared differences (*SSD*) between L and $\hat{L} = K \cdot \hat{C}$. In practice, only the TACs of the 14 outer layers are considered in the following. Figure 3 shows the layer and the compartment TACs for subject #530.

2.4 Model parameter estimation

In this section, we describe the different steps to estimate the five transfer parameters (k_{01}, k_{02}, k_{12}, k_{21}, and k_{10}) that best describe the ^{99m}Tc-pertechnetate uptake phenomenon.

First, we need to mention that the direct analytic resolution of the inverse problem was eliminated, since it required to approximate all observations with a sum of four negative exponential functions. Such an approximation is highly unstable and not reliable.

Consequently, an indirect approach was chosen: the model transfer parameters are estimated by solving numerically the inverse problem from longitudinal observations [13]. The approach is decomposed into three steps:

1. We explored a large set of values for the transfer parameter values k_{ij}. All combinations of the k_{ij} values: $\{5 \times 10^{-3}, 10^{-1}, 5 \times 10^{-1}, 5\}$ were explored.
2. The downhill simplex algorithm [14] was performed once on the perturbated set of best six sets of parameters of the step 1.

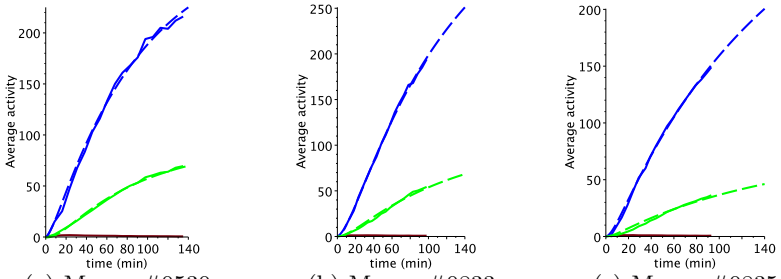

(a) Mouse #0530 (b) Mouse #0833 (c) Mouse #0835

Fig. 4. Compartment TAC and their approximate functions after downhill simplex optimisation. $\hat{\text{TAC}}_{\mathbf{W}}$ for the wall (blue continuous line) and $\hat{\text{TAC}}_{\mathbf{C}}$ for the cavity (green continuous line), and their approximate functions $\tilde{\text{TAC}}_{\mathbf{W}}$ (blue dashed line) and $\tilde{\text{TAC}}_{\mathbf{C}}$ (green dashed line).

3. The downhill simplex algorithm was performed a second time on the simplex made of six perturbations of the best set of parameters at step 2.

For each set of transfer parameters, the resulting estimated $\tilde{\text{TAC}}_{\mathbf{Layers}}$, $\tilde{\text{TAC}}_{\mathbf{Wall}}$ and $\tilde{\text{TAC}}_{\mathbf{Cavity}}$ were compared with the observed TACs: $\hat{\text{TAC}}_{\mathbf{Layers}}$, $\hat{\text{TAC}}_{\mathbf{Wall}}$ and $\hat{\text{TAC}}_{\mathbf{Cavity}}$. The comparison is performed according to the sum: $SSD_{\mathbf{Wall}} + SSD_{\mathbf{Cavity}}$. Finally, the mean relative errors (MRE) were computed on the wall TAC, the cavity TAC, and the layer TACs. When a best approximation is to be chosen, we choose the one with the lowest value for $SSD_{\mathbf{Wall}} + SSD_{\mathbf{Cavity}}$.

3 Results

We estimated the transfer parameters for five different subjects, we present below the results of these experiments. Figure 4 presents the resulting estimated compartment TACs for the wall ($\tilde{\text{TAC}}_{\mathbf{W}}$) and the cavity ($\tilde{\text{TAC}}_{\mathbf{C}}$) (dashed curves) together with the ones obtained from the observed TACs, $\hat{\text{TAC}}_{\mathbf{W}}$ and $\hat{\text{TAC}}_{\mathbf{C}}$ (continuous curves) for three subjects. Qualitatively, the estimated $\tilde{\text{TAC}}_{\mathbf{W}}$ (blue dashed line) fits nicely the observed $\hat{\text{TAC}}_{\mathbf{W}}$ and so does the estimated $\tilde{\text{TAC}}_{\mathbf{C}}$ (green dashed line) with $\hat{\text{TAC}}_{\mathbf{C}}$. Thus, from a qualitative point of view, the estimation of the transfer parameters is satisfying.

The set of transfer parameters after the whole process are presented in Table 1. For all subjects, the values for parameters k_{01}, k_{02} and k_{10} are in coherence. But the range of value for the parameters k_{12} and k_{21} is larger. The difference between estimated and observed TACs for both compartments is measured by the mean relative errors (MRE): $MRE = \frac{\Sigma_{observations \neq 0}(\frac{|Measures - Estimations|}{|Measures|})}{nb\ of\ observations}$. The MREs exhibit good results: around 5% for the wall, and less than 10% over the first 14 layers. Concerning the cavity, the MREs are more important with value up to 22% of error. This is due to the fact that the activity is lower in the cavity

Table 1. Transfer parameters for all the subjects and mean relative errors between the observations and the estimations. Results after the second execution of the downhill simplex algorithm.

	Transfer parameters					Mean relative error (%)		
Case	k_{01}	k_{02}	k_{12}	k_{21}	k_{10}	$MRE_{\mathbf{W}}$	$MRE_{\mathbf{C}}$	$MRE_{\mathbf{L}}$
0530	0.0050	-0.0140	0.1599	0.0466	2.0676	4.628	5.037	5.664
0833	0.0004	-0.0017	0.5839	0.1603	2.5757	1.538	8.627	5.063
0834	0.0081	-0.0396	1.2071	0.2465	2.5527	3.153	14.80	6.235
0835	0.0085	-0.0411	1.8594	0.4193	2.1931	4.676	22.40	9.645
0836	0.0037	-0.0424	0.1977	0.0418	1.9524	5.263	14.74	8.094

and that the optimisation criteria was not the minimisation of the mean relative error.

Overall, our results on the transfer parameters are coherent and excellent given the difficulty of the analysis and the simplicity of the model. This shows that our model is relevant. The values suggest that there is a mechanism of iodide exchange between the wall and the cavity of the stomach. However, the large discrepancy of values for k_{21} and k_{12} is not sufficient to understand the exchange mechanism. This is due to the approximations that we have made, and to the simplicity of model.

4 Discussion and Perspectives

In this article, we established a methodological approach based on compartmental analysis for the modelling of the ^{99m}Tc-pertechnetate uptake in the murine stomach. The aim was to study the iodide retention phenomenon in the stomach wall. As it was the first study of this kind, we chose a simple model and made several approximations. The results corroborate the iodide retention in the stomach wall and prove the relevance of our simplified model as well as the feasibility of the approach. However, the chosen model is not detailed enough to explain accurately all the details of the phenomenon of iodide retention. A more accurate analysis of the iodide exchange mechanism between wall and cavity requires a more complex model, that will most probably extend the first promising results presented in this paper. Such an extension together with a complete evaluation of the robustness should be addressed in future works.

The originality and strength of this work lies in the following contributions:

- A compartmental model of the stomach that distinguishes the stomach wall from the stomach cavity;
- An original decomposition of the stomach into layers, robust to deformation and progressive uptake;
- A numerical resolution methodology for determining the TACs for each compartment of the stomach;
- Finally, the computation of the parameters that characterise ^{99m}Tc-pertechnetate uptake in the stomach such that the behaviour of the model fits with the observations.

Even if further developments and probably refinements of the methodology will be necessary to improve the robustness of the results and the precision of the stomach model, the presented results are beyond our expectations because the method allows us to compute transfer parameters that are coherent between the different subjects.

Acknowledgement

This section will be written later in order to preserve anonymity.

References

1. Lathrop, K., Harper, P.: Biologic behavior of 99m Tc from 99m Tc-pertechnetate ion. Progress in nuclear medicine **1** (1972) 145
2. Hofmeyr, N.: Stomach scanning after intravenous 99mTc administration. A preliminary report. South African medical journal/Suid-Afrikaanse tydskrif vir geneeskunde **41**(23) (1967) 572
3. Franken, P.R., Guglielmi, J., Vanhove, C., Koulibaly, M., Defrise, M., Darcourt, J., Pourcher, T.: Distribution and dynamics of 99m Tc-Pertechnetate uptake in the thyroid and other organs assessed by single-photon emission computed tomography in living mice. Thyroid **20**(5) (2010) 519–26
4. Reutter, B.W., Gullberg, G.T., Huesman, R.H.: Direct least-squares estimation of spatiotemporal distributions from dynamic SPECT projections using a spatial segmentation and temporal B-splines. **19**(5) (May 2000) 434–50
5. Jiao, J., Searle, G., Tziortzi, A., Salinas, C., Gunn, R., Schnabel, J.: Spatial-temporal Pharmacokinetic Model Based Registration of 4D Brain PET Data. In Durrleman, S., Fletcher, T., Gerig, G., Niethammer, M., eds.: Spatio-temporal Image Analysis for Longitudinal and Time-Series Image Data. Volume 7570 of Lecture Notes in Computer Science. Springer Berlin Heidelberg (2012) 100–12
6. Nioche, C., Soret, M., Gontier, E., Lahutte, M., Dutertre, G., Dulou, R., Capelle, L., Guillevin, R., Foehrenbach, H., Buvat, I.: Evaluation of quantitative criteria for glioma grading with static and dynamic 18F-FDopa PET/CT. Clinical nuclear medicine **38**(2) (2013) 81–7
7. Jacquez, J.: Compartmental analysis in biology and medicine. BioMedware (1996)
8. Fresen, J., Juritz, J.: A note on Foss's method of obtaining initial estimates for exponential curve fitting by numerical integration. Biometrics **42**(4) (1986) 821–827
9. Otsu, N.: A Threshold Selection Method from Gray-Level Histograms. **9**(1) (1979) 62–66
10. Zang, Y., Jiang, T., Lu, Y., He, Y., Tian, L.: Regional homogeneity approach to fMRI data analysis. NeuroImage **22**(1) (May 2004) 394–400
11. Borgefors, G.: Distance transformations in digital images. Computer Vision, Graphics, and Image Processing **34**(3) (1986) 344–71
12. Penrose, R.: A generalized inverse for matrices. Proc. Cambridge Philos. Soc **51**(July) (1955) 406–413
13. Rubinow, S., Winzer, A.: Compartment analysis: an inverse problem. Math. Biosci. **11** (1971) 203–247
14. Press, W., Teukolsky, S., Vetterling, W., Flannery, B.: Numerical recipes in C: the art of scientific computing. In: Downhill Simplex Method in Multidimensions. 2nd edn. Cambridge University Press, Cambridge, UK (oct 1992) 402–412